Chemical Engineering Journal 342 (2018) 61–70

Contents lists available at ScienceDirect

Chemical Engineering Journal

journal homepage: www.elsevier.com/locate/cej

Mass transfer intensification in a novel airlift reactor assembly with helical sieve plates

Zhiyong Zheng[a,b,*], Yuqi Chen[a], Xiaobei Zhan[a,*], Minjie Gao[a], Zifan Wang[a]

[a] Key Laboratory of Industrial Biotechnology of Ministry of Education, School of Biotechnology, Jiangnan University, Wuxi 214122, China
[b] Jiangsu Key Laboratory of Anaerobic Biotechnology, School of Environment and Civil Engineering, Jiangnan University, Wuxi 214122, China

HIGHLIGHTS

- A novel airlift reactor assembly with helical sieve plates was developed.
- Gas holdup and volumetric mass transfer coefficient were significantly intensified.
- Helical sieve plate structure and reactor performance were related to each other.
- Bubble size decreased and its distribution in the reactor was narrow.

GRAPHICAL ABSTRACT

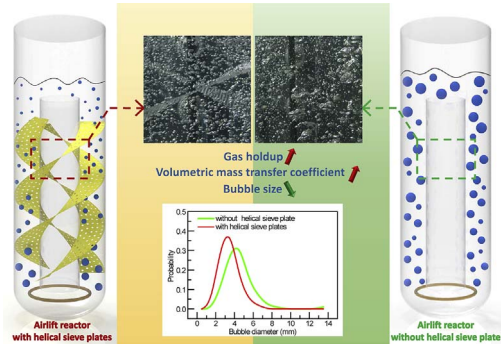

ARTICLE INFO

Keywords:
Bioreactor
Gas holdup
Mixing
Bubble sizes
Bubble breakup

ABSTRACT

A novel airlift reactor (ALR) assembly with helical sieve plates (HSPs) in the riser section was developed to intensify gas–liquid mass transfer process. The mass transfer and mixing characterization of the ALR assembly with different HSP structures was analyzed and compared using gas holdup, volumetric mass transfer coefficient, bubble velocity, and mixing time as assessment parameters. With optimized HSP, the gas holdup and volumetric mass transfer coefficient of the reactor were significantly increased by 38–53% and 76–144%, respectively, compared with those of the classical ALR. The empirical equations of gas holdup and volumetric mass transfer coefficient in the new ALR under the experimental condition were proposed. With the increase in the free area ratio in the HSP, a large number of bubbles were broken into small bubbles. Thereafter, the gas–liquid mass transfer efficiency was improved by increasing the gas–liquid interfacial area. Large helix angle caused part of the bubbles to flow helically. As a result, the circumferential mixing of fluid was enhanced whereas the overall mixing time was shortened.

1. Introduction

Airlift bioreactor is developed on the basis of a bubble column reactor and used for gas–liquid or gas–liquid–solid multiphase flow reactions [1,2]. It exhibits better mixing performance than that of bubble column reactor. Moreover, it possesses several advantages, such as simple structure, insensitivity to microbial contamination, energy saving property, and low shear stress, compared with mechanical agitated reactor [3,4]. Airlift reactor (ALR) is widely used in biological aeration in wastewater treatment, aerobic fermentation, and Fischer–-Tropsch synthesis [5–7].

Given the narrow operational flexibility and relatively low mass transfer rate of ALR, the aerobic fermentation process is dominated by mechanical agitated reactor [8,9]. To promote the mass transfer and

* Corresponding authors at: Key Laboratory of Industrial Biotechnology of Ministry of Education, School of Biotechnology, Jiangnan University, Wuxi 214122, China (Z. Zheng).
E-mail addresses: zhiyong@jiangnan.edu.cn (Z. Zheng), xbzhan@jiangnan.edu.cn (X. Zhan).

https://doi.org/10.1016/j.cej.2018.01.039
Received 7 November 2017; Received in revised form 6 January 2018; Accepted 6 January 2018
Available online 11 January 2018
1385-8947/

Nomenclature

a	Gas–liquid interfacial area, m^2/m^3
C_L	Dissolved oxygen concentration indicated by a probe, %
C_0	Initial concentration of dissolved oxygen, %
C^*	Saturated concentration of dissolved oxygen, %
D	Reactor diameter, m
D_L	Molecular diffusion coefficient, m^2/s
d	Equivalent diameter of bubble, m
d_{32}	Sauter mean diameter of bubble, m
d_s	Screen diameter, mm
E	Major axis of an ellipse, m
e	Minor axis of an ellipse, m
h_L	Liquid level before aeration, m
h_D	Liquid level during aeration, m
k_La	Volumetric mass transfer coefficient, 1/s
k_L	Liquid-side mass transfer coefficient, m/s
L	Length of bubble displacement, m
N	Number of screen, –
n	Flow behavior index, –
P_G/V_D	Pneumatic power input per unit gas-liquid dispersion volume, W/m^3
p	Probability value, –
R_{adj}^2	Adjusted R-square, –
Re_b	Bubble Reynolds number, –
S	Projected area of bubble, m^2
T	Water temperature, ˚C
t	Time, s
U_g	Superficial gas velocity, m/s
U_{slip}	Velocity difference between bubble and liquid, m/s
V	Bubble velocity, m/s
V_A	Resultant velocity, m/s
V_x	Circumferential velocity component, m/s
V_L	Liquid velocity, m/s
V_y	Axial velocity component, m/s

Greek

β	Direction angle of bubble displacement, ˚
ε	Overall gas holdup, %
θ	Helix angle
μ_L	Liquid viscosity, Pa·s
ρ_L	Liquid density, kg/m^3
τ	Probe response time, s
ω	Free area ratio, %

Abbreviations

ALR	Airlift reactor
ALR-HSP	Airlift reactor assembly with helical sieve plates
HSP	Helical sieve plate
OSP	Horizontal sieve plate
OWM	Horizontal wire mesh

energy-saving performance of ALR, researchers have developed several gas spargers [10,11] and optimized reactor structures [12]. Zimmerman et al. [13] developed a fluidic oscillator that significantly reduces bubble diameter by using air pulses. Although the novel sparger can decrease the initial size of bubble, the bubble coalescence during rise for submerged cultivation is still not solved. Researchers have installed static mixers [14,15], horizontal sieve plates (OSPs) [16,17], impellers [18], and vibrating apparatuses [19] in the bubble column and ALR to prevent the bubble coalescence. ALR assembly with OSPs in the riser section can enhance the breakup of bubbles and improve the efficiency of mass transfer [16]. Although OSP promote gas holdup at low aeration rate, the volumetric mass transfer coefficient cannot be increased in accordance with the increase in gas holdup at high aeration rate. This condition is due to that bubbles accumulate under the OSP and gas blocking occurs. In addition, multi-layer OSPs installed in the bubble column are difficult to be accessed and cleaned and are thus undesirable for biological reaction and aerobic fermentation.

Bubble size and gas holdup determine the specific gas–liquid interface surface area, which significantly affects the volumetric mass transfer coefficient. Unfortunately, no fairly rigorous theory of bubble breakup processes exists. In recent years, several researchers have studied the breakup and coalescence of bubble in the reactor [20–22]. They have speculated that bubble breakup is due to the abrupt acceleration of liquid, influence of stresses on a bubble in the gradient field, effect of turbulent pulsations, and development of instability of the interface boundary [23]. High pressure can be beneficial in reducing bubble size, improving the driving force for mass transfer and inhibiting bubble swarm, thereby improving gas–liquid mass transfer efficiency [24]. Ramezani et al. [25] found that although surfactant (ethanol) addition can decrease the surface tension and result in smaller bubble sizes, the diffusion coefficient may also be reduced which leading to a decrease in liquid-side mass transfer coefficient (k_L). Bubble size and its distribution influence the transition of the flow regime [26]. Therefore, the size and shape of bubble in the bubble column is dependent not only on the superficial gas velocity of gas but also on the turbulence and instability of bubble.

The interphase mass transfer and their characteristics are crucial for evaluating the performance of the airlift reactors. Predicting gas holdup (ε) and volumetric mass transfer coefficient (k_La) of an airlift reactor through empirical correlations is vital for optimization and scale-up of the reactor. The empirical correlations reported in literatures and their operational conditions are briefly summarized in Table 1.

A novel airlift reactor assembly with helical sieve plates (ALR-HSP) was developed in our previous work [31]. The current study aimed to determine the relationship between the HSP structure and the mass transfer characteristics of the ALR. It would help to provide a framework for establishing scale-up correlation equations for reactor design and facilitating this novel reactor in industrial applications, such as aerobic fermentation and biological aeration.

2. Materials and methods

2.1. Experimental setup

The experiment was carried out in a 120 L internal-loop ALR, which was composed of a cylindrical tank and a stainless-steel elliptic head (Fig. 1). The liquid volume was 95 L. A square transparent jacket was assembled outside of the tank, which was filled with water, to avoid the deformation of optical refraction when observing the bubbles in the tank. A plexiglass draft tube was installed in the tank center, which was supported by three legs. The gas sparger was looped by a steel pipe with a diameter of 300 mm, and 20 holes with a diameter of 1.5 mm were evenly distributed on it. The gas sparger was located horizontally at the bottom of the annulus (riser section) between the tank wall and draft tube. The inner-side of the draft tube was set as the downcomer section. Table 2 shows the detailed structure dimensions of the reactor.

The HSPs were made of 1.5 mm-thick transparent polycarbonate plastic, on which 5 mm holes were evenly arranged in a regular triangular pattern. The central distances between adjacent holes were 6 mm, 7 mm and 8 mm, corresponding to the free area ratios ω of 35%, 46% and 63%. The helix angles θ of the plates were 10˚, 20˚ and 31˚. Nine HSPs with different free area ratios and helix angles were fixed in the

Table 1
Summary on the empirical equations and the variables ranges in reactor.

Author	Reactor type	Empirical correlation	Operational condition
Bello et al. [27,28]	ILAR, ELAR	$\varepsilon = 3.4 \times 10^{-3}\left(\frac{P_G}{V_D}\right)^{2/3}\left(1+\frac{A_d}{A_r}\right)^{-1}$ $k_La = 5.5 \times 10^{-4}\left(\frac{P_G}{V_D}\right)^{0.8}\left(1+\frac{A_d}{A_r}\right)^{-1.2}$	Water, 0.15 kmol/m^3 NaCl solutions ILAR: A_d/A_r = 0.13, 0.35, 0.56 ELAR: A_d/A_r = 0.11–0.69 0.008 W/m^3 ≤ P_G/V_D ≤ 0.07 W/m^3
Kawase et al. [29]	ILAR, BC	$\varepsilon = 0.24\left(\frac{U_g}{\sqrt{gD}}\right)^{0.84-0.14n}\left(\frac{gDU_g\rho_L}{\mu_L^2}\right)^{0.07}$ $\frac{k_LaD^2}{D_L} = 0.68n^{-6.72}\left(\frac{DU_g\rho_L}{\mu_L}\right)^{0.38n+0.52}\left(\frac{\mu_L}{D_L\rho_L}\right)^{0.38n-0.14}$	Water, Pseudo-plastic fluid 0.008 m/s ≤ U_g ≤ 0.285 m/s ILAR, BC: 0.14 m ≤ D ≤ 0.35 m 0.28 ≤ n ≤ 1
Luo et al. [16]	ILAR	$\varepsilon = 107.72d_s^{0.19}\omega^{-0.16}N^{0.21}U_g^{0.75}$ $k_La = 0.35d_s^{0.19}\omega^{0.13}N^{0.48}U_g^{0.86}$	Water 0.877 × 10^{-3} m/s ≤ U_g ≤ 2.81 × 10^{-3} m/s 2.5 mm ≤ d_s ≤ 3.5 mm 1 ≤ N ≤ 2 0.37 ≤ ω ≤ 0.73
Räsänen et al. [11]	ALR	$\varepsilon = 0.0756 \pm 0.0023\left(\frac{U_{gsr}}{U_{gsr,avg}}\right)^{0.6929 \pm 0.0619}\left(1+\frac{U_{gsd}}{U_{gsd,avg}}\right)^{0.0165 \pm 0.0408}$ $k_La = 4.4773 \pm 3.1070U_{gs}^{1.3802 \pm 0.1847}$	Water 0.013 m/s ≤ U_{gs} ≤ 0.034 m/s
Zhang et al. [30]	ILALR	$\varepsilon = 0.34U_g^{0.705}$ (No screen) $\varepsilon = 0.325U_g^{0.75}[4.74-(3.35-d_s)^2]^{0.062}$ (With screen) $k_La = 8.34U_g^{0.339}[3.24-(2.99-d_s)^2]^{0.056}$ (With screen)	Water 1.2 mm ≤ d_s ≤ 4.75 mm 0.01 m/s ≤ U_g ≤ 0.06 m/s

riser of the reactor by using horizontal steel bars. The experiment was carried out in the room temperature. The superficial gas velocity (U_g) range was 0.009 – 0.09 m/s.

2.2. Measurements

2.2.1. Gas holdup

The volume of the gas phase in the liquid phase could be calculated by measuring the liquid level before and after aeration. The overall gas holdup ε was calculated as follows:

$$\varepsilon = \frac{h_D - h_L}{h_D} \quad (1)$$

where h_L is the liquid level before aeration, m. h_D is the liquid level during aeration, m.

2.2.2. Volumetric mass transfer coefficient

Volumetric mass transfer coefficient (k_La) was measured using the dynamic gassing-out–gassing-in method [32]. Two dissolved oxygen (DO) probes were mounted in the riser and downcomer sections, separately, at 0.510 m and 0.300 m up from the lower edge of the draft tube. The k_La in the riser and the downcomer was measured simultaneously. First, nitrogen was bubbled through the reactor at high gas velocity until the DO concentration (Mettler Toledo InPro 6800) was less than 5%. Then, nitrogen was stopped and air was injected into the reactor at a preset flow rate. The DO controller automatically collected data until it reached a level above 90%. Considering the response time of the DO probe and the water temperature, the volumetric mass transfer coefficient could be calibrated according to following equations:

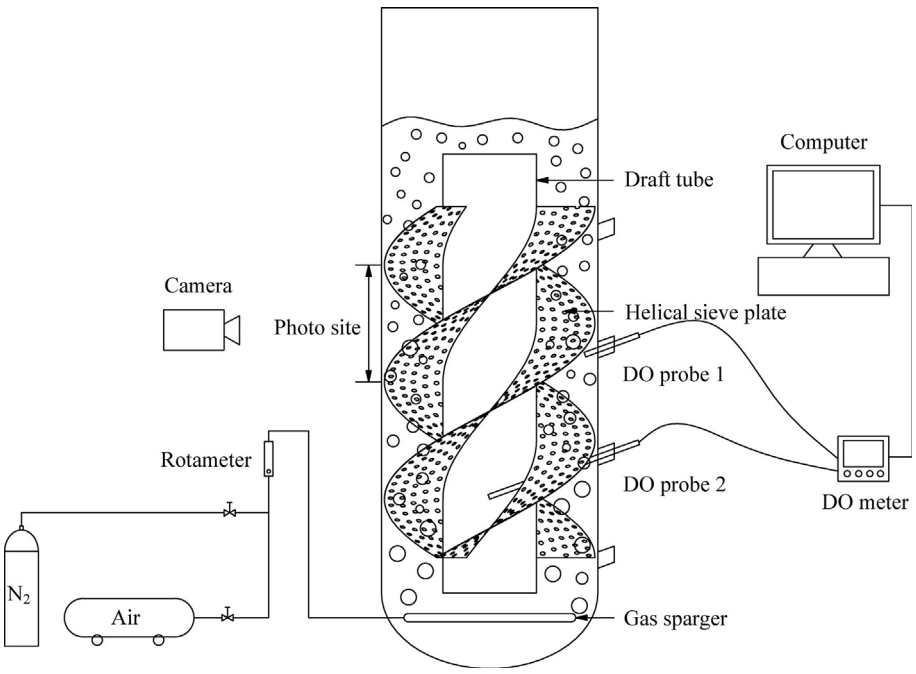

Fig. 1. Schematic of the experimental airlift reactor.

Table 2
Structure dimensions of the experimental reactor.

Dimension	Value
Tank height	1.130 m
Tank inner diameter	0.370 m
Draft tube height	0.750 m
Draft tube inner diameter	0.230 m
Draft tube outer diameter	0.240 m
Cross-sectional area ratio of downcomer to riser	0.693
Support leg height	0.100 m
HSP height	0.600 m
Distance between the lower edges of HSP and the draft tube	0.060 m
Spacing between adjacent HSPs	0.200 m

$$\frac{C^*-C_L}{C^*-C_0}=\frac{e^{-k_La\cdot t}-k_La\cdot\tau\cdot e^{-\frac{t}{\tau}}}{(1-k_La\cdot\tau)} \quad (2)$$

$$k_La(25)=\frac{k_La(T)}{1.024^{T-25}} \quad (3)$$

where C^* is the saturated concentration of dissolved oxygen, %; C_L is the dissolved oxygen concentration indicated by a probe, %; C_0 is the initial concentration of dissolved oxygen, %; t is the measuring time, s; τ is the dissolved oxygen probe response time, s; T is the water temperature, ˚C. The experiments were carried out at the room temperature. 25 ˚C was chose as the reference temperature and all the k_La data were calibrated.

2.2.3. Diameter and velocity of bubble

The diameter and velocity of bubble were measured by taking photos with a camera (Cannon EOS 500D) and then analyzing the images. The exposure time of the camera was set at 1/1000 s (quick shutter). The site of photo shooting was 0.200 × 0.100 m ($W \times H$) and its distance from the bottom of the reactor was 0.700 m. For the bubble shape similar to an ellipse, the major axis E and minor axis e were measured. The equivalent diameter of bubble was calculated according to Eq. (4). For irregularly shaped bubbles, the equivalent diameter was calculated according to Eq. (5) as follows:

$$d=\sqrt[3]{E^2e} \quad (4)$$

$$d=\sqrt{4S/\pi} \quad (5)$$

where S is the projected area of bubble, m^2.

The Sauter mean diameter d_{32} of bubble was calculated according to

$$d_{32}=\frac{\sum n_i d_i^3}{\sum n_i d_i^2} \quad (6)$$

where n_i is the number of bubbles; d_i is the equivalent diameter of each bubble, m.

Bubble velocity was obtained by calculating the bubble displacement in the photograph taken by the camera at a preset exposure time and at the same shooting site. The exposure time was set at 1/40–1/200 s (slow shutter) according to bubble velocity under different operating conditions. First, for the sake of reducing the number of observable bubbles and conveniently measuring the movement of bubbles in the reactor, an opaque blue plastic sheet was placed in the local area of the reactor along the circumferential direction on a cylindrical surface (r = 0.160 m). The trajectories of bubbles under various helical sieve plate conditions and various superficial gas velocities were recorded by the camera. Then, the displacement length L and the direction angle β of the bubbles in a fixed area of a rectangle were obtained (Fig. S1). Finally, the average resultant velocity V_A, the circumferential velocity component V_x ($=L\cdot\cos\beta/t$), and the axial velocity component V_y ($=L\cdot\sin\beta/t$) of bubbles were calculated. The number of bubbles calculated under each condition was between 300 and 400.

2.2.4. Mixing time

After the aeration condition was stabilized, 20 ml 1.0% (w/v) of phenolphthalein and 30 ml of 1.0 mol/L NaOH were added into the reactor. When the tracer agents were homogeneously mixed, the liquid became magenta in color. Thereafter, 30 ml 1.0 mol/L of HCl was added and the timer was started until the solution in the whole reactor was colorless. The resulting time was considered as the mixing time.

3. Results and discussion

3.1. Gas holdup

Gas holdup and bubble diameter determine the gas–liquid interfacial area (a), which significantly affects the mass transfer rate. Fig. 2 shows the relationship between the gas holdup and superficial gas velocity in the ALR assembled with nine different HSPs and without a sieve plate. Under the investigated conditions, gas holdup increased with the increase in superficial gas velocity, which was mainly dependent on gas flow rate. Gas holdup was obviously higher in ALR-HSP than that without sieve plate at the same superficial gas velocity. However, the effect of different HSP structures on gas holdup was not obvious. The HSPs mildly impeded the rising bubbles, helically moved partial bubbles, reduced the axial velocity, and lengthened the movement path. Thus, the overall gas holdup was improved. When free area ratio was 63% and helix angle was 31˚, gas holdup increased by 38–53% ($p \le 0.01$) more than that without sieve plate.

Bubble flow regimes can be categorized into homogeneous, transition, and heterogeneous flows according to certain characteristics, such as superficial gas velocities and bubble size distribution. For homogeneous flow, bubbles are evenly distributed and the interaction between bubbles and liquid flow is tender; on the contrary, for heterogeneous flow, the coalescence and breakup of bubble frequently occur and the interaction between the bubbles and liquid flow is intensive [33]. Fig. 2 shows that the increase in gas holdup in the reactor without sieve plate became slow when superficial gas velocity was at 0.072 m/s. Using the method proposed by Besagni and Inzoli [26], the curve of U_g/ε versus ε was plotted to evaluate the flow regime transition point based on swarm velocity. For the ALR without sieve plate, the transition point of the superficial gas velocity from the homogeneous regime to the heterogeneous regime was at 0.07 m/s. The transition point in the bubble column reported by Shah et al. [34] was 0.04–0.075 m/s. By contrast, for the ALR assembly with horizontal wire meshes (OWM with square holes) investigated by Zhang et al. [30], gas holdup increased slowly when superficial gas velocity reached 0.03–0.04 m/s, which was the transition point to the heterologous flow regime. However, for ALR-

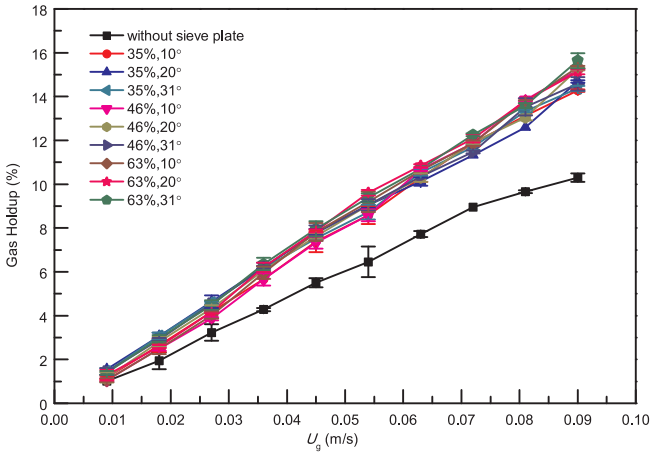

Fig. 2. Variation in gas holdup with superficial gas velocity in the airlift reactor assembly with different helical sieve plates. The first column in the legend is the free area ratio ω (%) and the second column is the helix angle θ (°).

HSP, the superficial gas velocity transition point did not emerge in the investigated ranges. It is implied that the HSP could allow the gas–liquid fluid to maintain a homogeneous flow regime over a wider range of superficial gas velocities and could show better operating performance and robustness than those of OWMs. Due to the impediment of the sieve plate or the wire mesh, gas-blocking might occur at high superficial gas velocity and result in an increase of gas holdup, whereas its impact on the mass transfer was probably determined by the type of plate and the free area ratio. For the case of gas-blocking led by horizontal baffles, it was not beneficial to the gas-liquid mass transfer [35].

As round hole was used in the HSPs in the present work, the maximum free area ratio could not exceed the theoretical value of 78.5%. Considering the limited manufacturing precision, the maximum free area ratio of 63% was adopted. The empirical correlation equations of gas holdup, derived from Zhang et al. [30], comprising superficial gas velocity, helix angle, and free area ratio were fitted with the least squares method as follows:

$$\varepsilon = 1.332U_g^{1.038} \quad \text{(without sieve plate)}$$
$$R^2_{adj} = 0.998 \tag{7}$$

$$\varepsilon = 1.766U_g^{1.009}\theta^{0.008}[0.85-(0.798-\omega)^2]^{0.199} \quad \text{(with HSP)}$$
$$R^2_{adj} = 0.996 \tag{8}$$

where U_g is the superficial gas velocity, m/s; θ is helix angle, °; ω is the free area ratio,%. The Eqs. (7) and (8) are valid over the ranges of the variables as follows:

$$0.009\ \text{m/s} \le U_g \le 0.09\ \text{m/s},$$
$$10^\circ \le \theta \le 31^\circ,$$
$$35\% \le \omega \le 63\%,$$

A good consistency was achieved between the experimental data and mathematical models with relative errors of less than 10%. The sensitivity coefficients of superficial gas velocity, helix angle, and free area ratio to gas holdup were 1.009, 0.007, and 0.041 respectively. Superficial gas velocity was the main factor that influenced gas holdup. The sensitivity of free area ratio was larger than that of helix angle.

For the bio-reaction process, limited oxygen transfer rate is commonly not beneficial to cell growth rate and cell density. It would further limit the product accumulation and result in high cost of product recovery. On the contrary, excessive oxygen transfer rate is not necessary for bio-reactions. On the one hand it would increase the gas holdup and then result in loss of the effective liquid volume and the product productivity in the reactor. On the other hand it would also result in the energy overconsumption. As for the airlift reactors, it would be preferable to have a wider range to meet the operation flexibility for the various bio-reaction systems. Therefore, we pursue a higher oxygen transfer rate in order to promote the operational robustness and applicability of the reactor.

3.2. Volumetric mass transfer coefficient

Volumetric mass transfer coefficient k_La is a key parameter for the gas–liquid mass transfer process and is the product of liquid-side mass transfer coefficient k_L and gas–liquid interfacial area a. According to the two-film theory, the interfacial area of gas–liquid is related to gas holdup and bubble size while the liquid-side mass transfer coefficient is related to the "thickness" of the liquid film, which is further related to the relative velocity of gas–liquid motion and physical properties of the gas–liquid two-phase (such as viscosity, diffusibility, surface tension and density).

The effects of different HSP structures (θ and ω) on k_La in the ALR were investigated. Fig. 3 shows that k_La increased with the increase in superficial gas velocity U_g. k_La remarkably increased in ALR-HSP compared with that in the classical ALR at the same U_g. Fig. 3a, b and c show the effect of different values of ω on k_La in the riser section under fixed helix angle. k_La increased with the increase in ω. With the increase in ω, bubbles rose vertically and were cut and broken into small bubbles. As a result, the gas–liquid interfacial area was improved, thereby strengthening the gas–liquid mass transfer. When superficial gas velocity reached 0.072 m/s, k_La was no longer increased under the condition of without sieve plate and ALR-HSP with ω = 63%. Therefore, the gas–liquid flow would reach a heterologous churn-turbulent regime at high superficial gas velocity and resistance in vertical direction would be less. However, when free area ratio was relatively low, the heterologous churn-turbulent flow regime would be postponed and the linear section of k_La versus U_g would be elongated. The gas–liquid flow tended

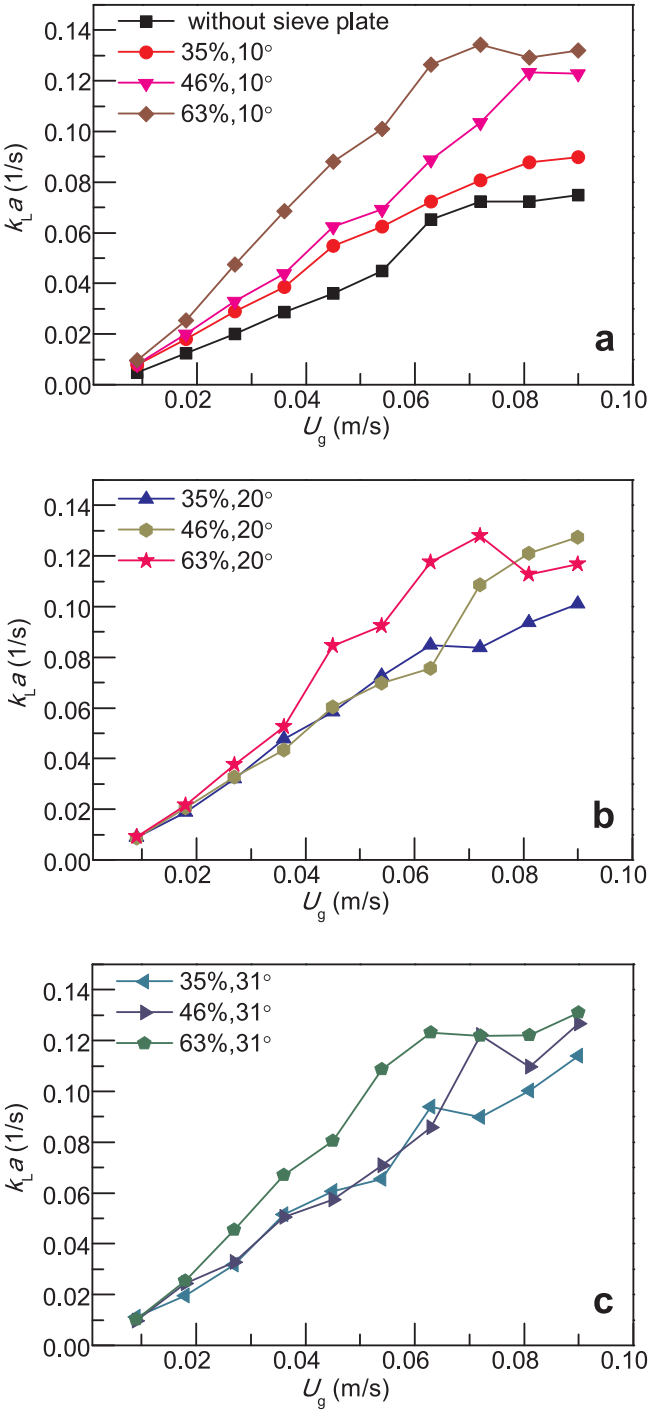

Fig. 3. Variation in k_La in the riser section with superficial gas velocity under different sieve plate conditions. (a) θ = 10°; (b) θ = 20°; (c) θ = 31°.

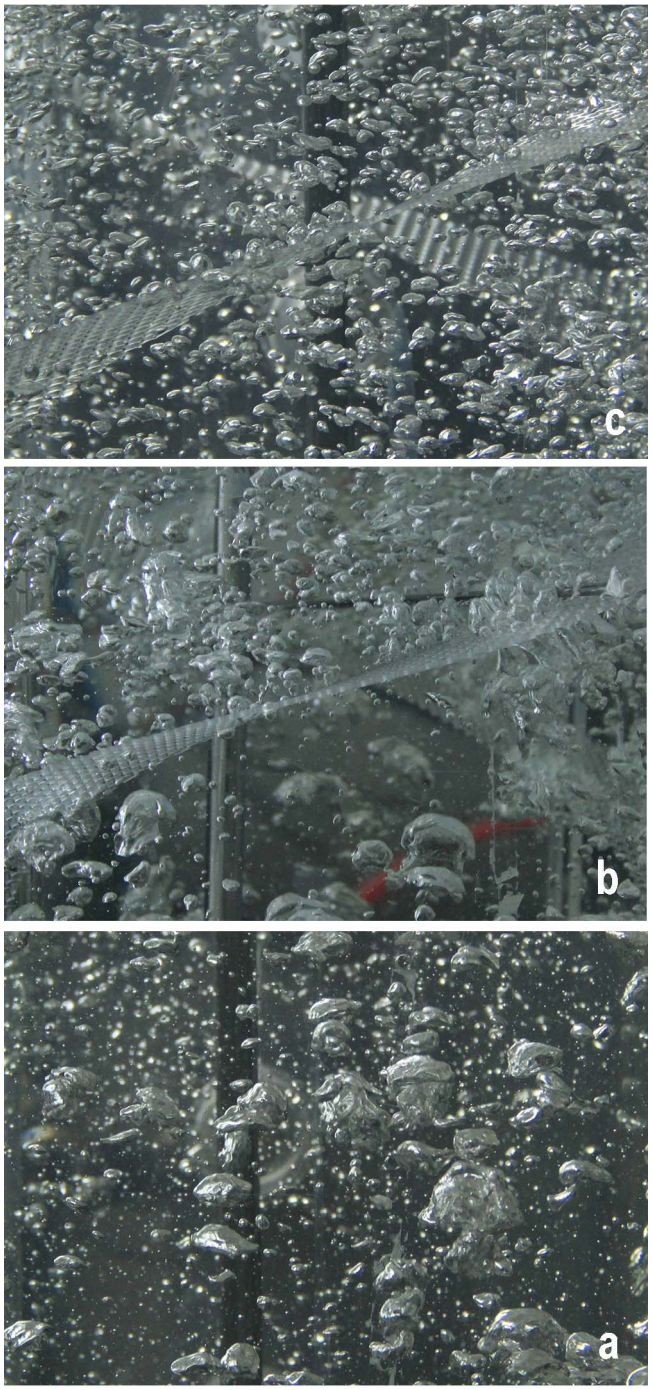

Fig. 4. Bubble size distributions and shapes in the various local zones of the airlift reactor. (a) Without helical sieve plate; (b) Bubbles go through the helical sieve plate for the first time; (c) Bubbles go through the top helical sieve plate.

to rise helically owing to the existence of the HSP with low ω. According to θ, the operational flexibility of ALR-HSP was broadened.

Fig. 3 shows that, for ω = 35% in the HSP, k_La was influenced by various helix angles θ; by contrast, for high ω, k_La was slightly dependent on θ. k_La increased by 76–144% ($p \leq 0.01$) in ALR-HSP under the optimized condition (θ = 10°, ω = 63%) with various superficial gas velocities than that without sieve plate. Helix angle was low while gas–liquid fluid flowed vertically. Most of the bubbles went through the HSP and were broken by the sieve pores. For the ALR assembly with OSPs [16], k_La increased by 50–80% more than that of ALR without sieve plate. The k_La depends not only on the turbulence of the gas-liquid flow, but also on the size, shape and distribution of the bubbles.

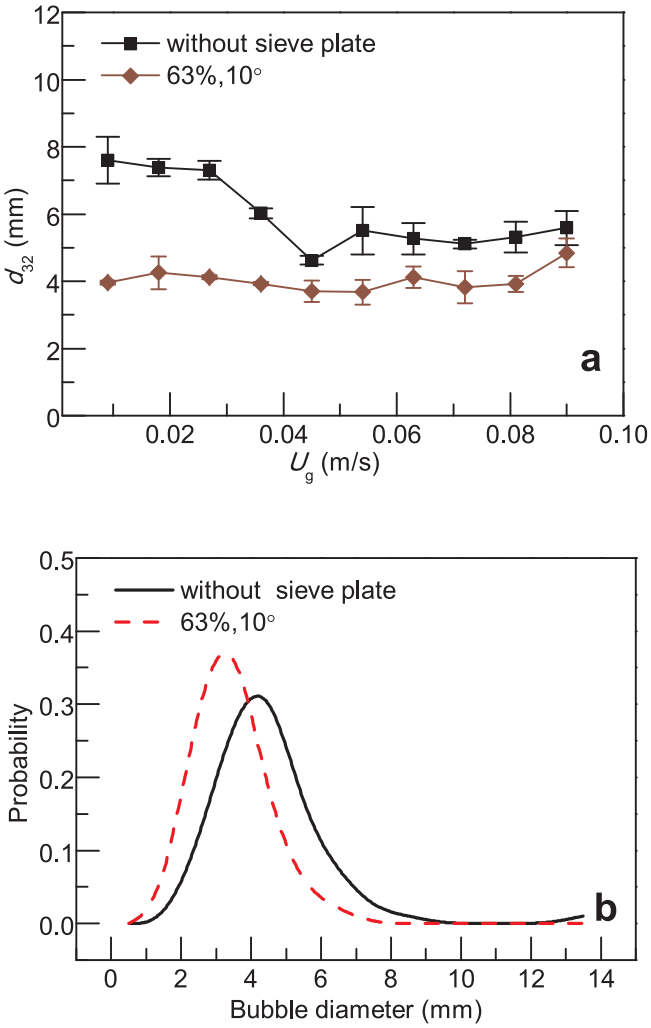

Fig. 5. Sauter mean diameter of bubble (a) and size distribution of bubble (b) in the ALR-HSPs and without sieve plate when U_g = 0.009 m/s.

Fig. 4 shows that the instantaneous shape of bubbles in the riser section of the ALR by using a camera. Fig. 4a shows the shape of bubbles in the ALR without sieve plate (the detection position was approximately 0.700 m above the bottom of the reactor). Partial bubbles were large and bubble size distribution was very wide. Fig. 4b shows that the bubbles went right through the HSP for the first time. From comparing the bubbles beneath and above the HSP, the average size of bubbles above the HSP was found to significantly reduce. Fig. 4c shows that the bubbles went through the top of the HSP. Nearly all bubbles were small and evenly distributed. They were frequently broken and became small every time they went through the plate. Fig. 5 shows the Sauter mean diameter (d_{32}) and size distribution of bubbles in ALR-HSP (ω = 63%, θ = 10°) and in the ALR without sieve plate for comparison. The Sauter mean diameter of bubbles (Fig. 5a) in ALR-HSP was obviously reduced. According to the bubble diameter distribution (Fig. 5b) at U_g = 0.009 m/s, the mathematical expectations were 3.43 and 4.47 while the variances were 0.96 and 2.31 for ALR-HSP and without sieve plate, respectively. Bubble size was evenly distributed and concentrated in a narrow range after going through the sieve plate.

Gas–liquid interfacial area a was calculated using Eq. (9), and liquid-side mass transfer coefficient k_L was obtained by dividing k_La by a.

$$a = \frac{6\varepsilon}{d(1-\varepsilon)} \tag{9}$$

Fig. 6 shows that a was increased significantly whereas k_L was nearly unchanged between ALR-HSP and ALR without sieve plate. The

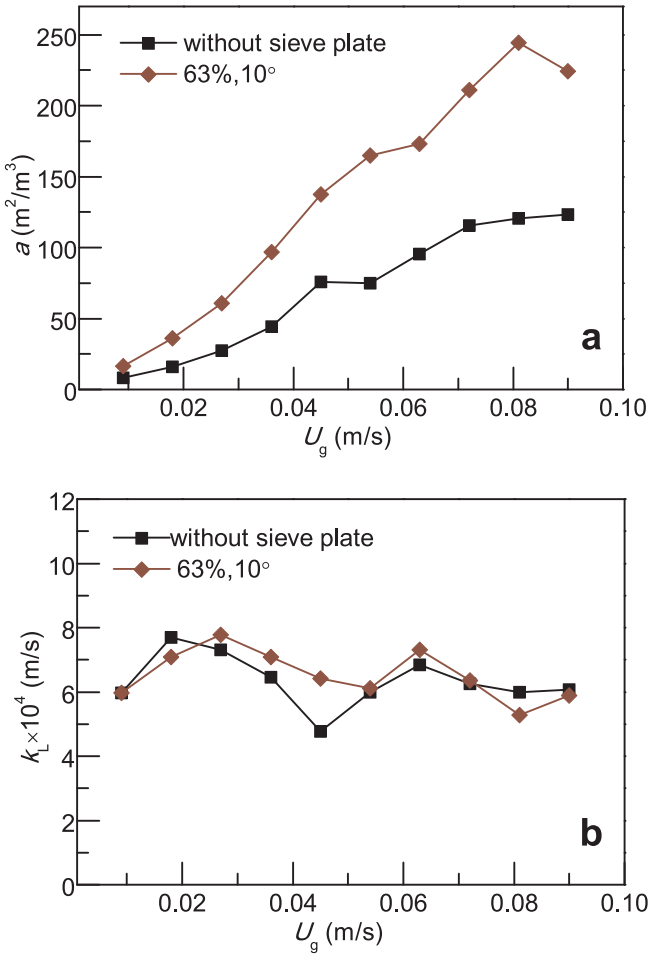

Fig. 6. Gas–liquid interfacial area a (a) and liquid-side mass transfer coefficient k_L (b) in the ALR-HSPs and without sieve plate.

decrease in the average diameter of bubbles and the increase in gas holdup resulted in a significant enhancement in a and thus the improvement in k_La in ALR-HSP.

Gas–liquid interfacial area a increases with decreasing bubble diameter. When the bubble diameter d is larger than 1.0 mm, bubble rising

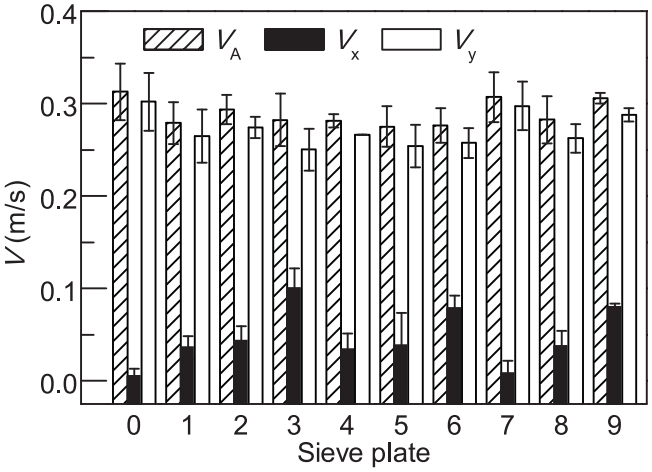

Fig. 7. Bubble rising velocity in the riser section with different helical sieve plates. V_A: resultant velocity, V_X: circumferential velocity component, and V_y: axial velocity component. U_g = 0.027 m/s. Number in the horizontal ordinate refers to the sieve plate structure: (0) without sieve plate; (1) ω = 35%, θ = 10°; (2) ω = 35%, θ = 20°; (3) ω = 35%, θ = 31°; (4) ω = 46%, θ = 10°; (5) ω = 46%, θ = 20°; (6) ω = 46%, θ = 31°; (7) ω = 63%, θ = 10°; (8) ω = 63%, θ = 20°; (9) ω = 63%, θ = 31°.

velocity and liquid velocity would not change obviously with bubble diameter [36,37]. Therefore, the velocity difference between bubble and liquid ($U_{slip} = |V - V_L|$) and k_L are not obvious changed. The increase of k_La is mainly due to the increase of a at the condition of $d > 1.0$ mm rather than the k_L. However, when $d < 1.0$ mm, the bubble rising velocity decreases with the smaller bubble diameter [37]. It resulted in the smaller velocity difference (U_{slip}), decreasing of bubble Reynolds number (Re_b) and liquid-side transfer coefficient k_L. So the k_La might have a threshold value (upper limit) in the range of $d < 1.0$ mm, i.e., smaller diameter bubbles do not necessarily result in a higher k_La.

Since the airlift reactor is mainly divided into the riser and the downcomer, the k_La in the riser is generally higher than that of in the downcomer. In order to distinguish the mass transfer differences between the riser and the downcomer. k_La in the downcomer section in ALR-HSP was also measured (data not shown) and was lower than that in the riser section. When bubbles passed through the gas–liquid separation zone, most of the bubbles in the riser section were drained off at the liquid level and a fraction of the small bubbles were carried into the downcomer section which resulted in low k_La. The overall k_La in the entire reactor could be calculated according to the cross-sectional area ratio of downcomer to riser. The overall k_La was slightly lower than k_La in the riser section. The experimental correlation equations of k_La in the riser and downcomer sections and overall ALR comprising superficial gas velocity, helix angle, and free area ratio were fitted with the least squares method as follows:

For the ALR without sieve plate,

$$k_La = 1.697U_g^{1.234} \quad \text{(riser)}$$
$$R^2_{adj} = 0.991 \tag{10}$$

$$k_La = 1.262U_g^{1.240} \quad \text{(downcomer)}$$
$$R^2_{adj} = 0.974 \tag{11}$$

$$k_La = 1.512U_g^{1.234} \quad \text{(overall)}$$
$$R^2_{adj} = 0.992 \tag{12}$$

For the ALR with sieve plates,

$$k_La = 1.989U_g^{0.958}\theta^{0.018}[0.798-(0.778-\omega)^2]^{1.42} \quad \text{(riser)}$$
$$R^2_{adj} = 0.946 \tag{13}$$

$$k_La = 1.722U_g^{1.098}\theta^{0.078}[0.798-(0.778-\omega)^2]^{1.037} \quad \text{(downcomer)}$$
$$R^2_{adj} = 0.931 \tag{14}$$

$$k_La = 1.869U_g^{1.005}\theta^{0.039}[0.798-(0.778-\omega)^2]^{1.285} \quad \text{(overall)}$$
$$R^2_{adj} = 0.956 \tag{15}$$

Research on the ALR assembly with OSP has shown that excess free area ratio is not beneficial for k_La because bubbles will be re-coalesced instantaneously when they leave the sieve plate [30]. In the present study, the effect pattern of free area ratio on k_La in ALR-HSP was similar to that in the ALR assembly with multi-layer OSPs. A good consistency was achieved between the experimental data and mathematical models with relative errors of less than 15%. The sensitivity coefficients of superficial gas velocity U_g, helix angle θ, and free area ratio ω to k_La in the riser section of ALR-HSP were 0.956, 0.018, and 0.707 respectively. The sensitivity of ω to k_La was higher than that to gas hold up, which meant that the influence of ω on k_La was more remarkable than that of gas hold up.

3.3. Bubble rising velocity

The moving trajectories of bubbles were recorded using the camera with preset exposure shooting. Although introducing the sheet would impede the radial flow of fluid, the circumferential velocity of bubbles

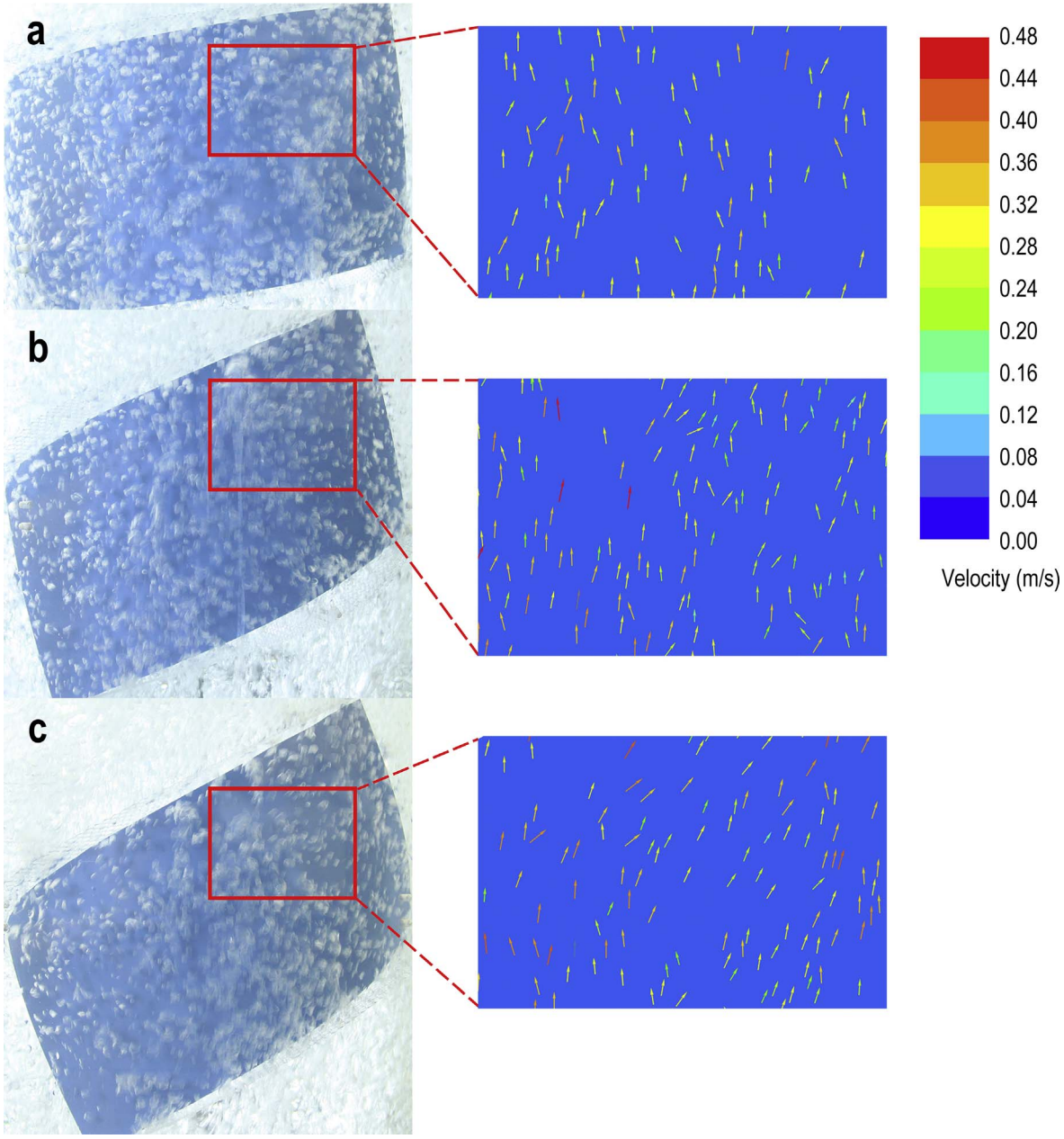

Fig. 8. Local bubble velocity in the airlift reactor with different helix angles when ω = 63% and exposure time was 0.0125 s. (a) θ = 10°; (b) θ = 20°; (c) θ = 31°.

would not be interfered obviously. Fig. 7 shows that the bubble velocities in the riser section of ALR-HSP were measured at a superficial gas velocity of 0.027 m/s. In general, the resultant velocity V_A was slightly larger than that without sieve plate. However, for HSPs with different structures, the difference was not obvious. V_x and V_y are the circumferential and axial velocity components, respectively, of the resultant velocity. The axial velocity was close to the resultant velocity and much larger than the circumferential velocity.

The circumferential velocity V_x increased obviously with the increase in helix angle, which further showed that increasing the helix angle would alleviate the impact of gas blocking. Meanwhile, as free area ratio increased, circumferential velocity V_x decreased slightly. When free area ratio was at low level, the resistance of the gas–liquid fluid going through the plate was not negligible and bubbles accumulated under the plate and formed gas blocking. The bubbles under the sieve plate rose helically when helix angle increased. For low free area ratio, k_La would increase with helix angle; by contrast, for high free area ratio, k_La was barely affected by helix angle (Fig. 3).

Fig. 8 shows that the recorded bubble flow pattern in ALR-HSP with different helix angles. With the increase in helix angle, bubbles freely moved helically. The bubbles in the center of the reactor were found to rise faster than did the bubbles in the peripheral region. Large bubbles with high velocity would produce an eddy flow and disturb the movement of the adjacent small bubbles. This phenomenon prominently occurs at high superficial gas velocity as described by Zhang [30]. For ALR-HSP, the interference intensity was increasingly obvious with the increase in helix angle in the current study.

In the present investigated airlift reactor, as shown in Fig. S2, the bubble rising velocity does not change manifestly with the superficial gas velocity. Due to the bubble breakup by the helical sieve plates, the bubble sizes were mainly distributed in the range of 1.0–8.0 mm and the bubble shapes were spherical or elliptical. The relationship between the bubble size and bubble rising velocity is consistent with the model reported by Bhole et al. [36].

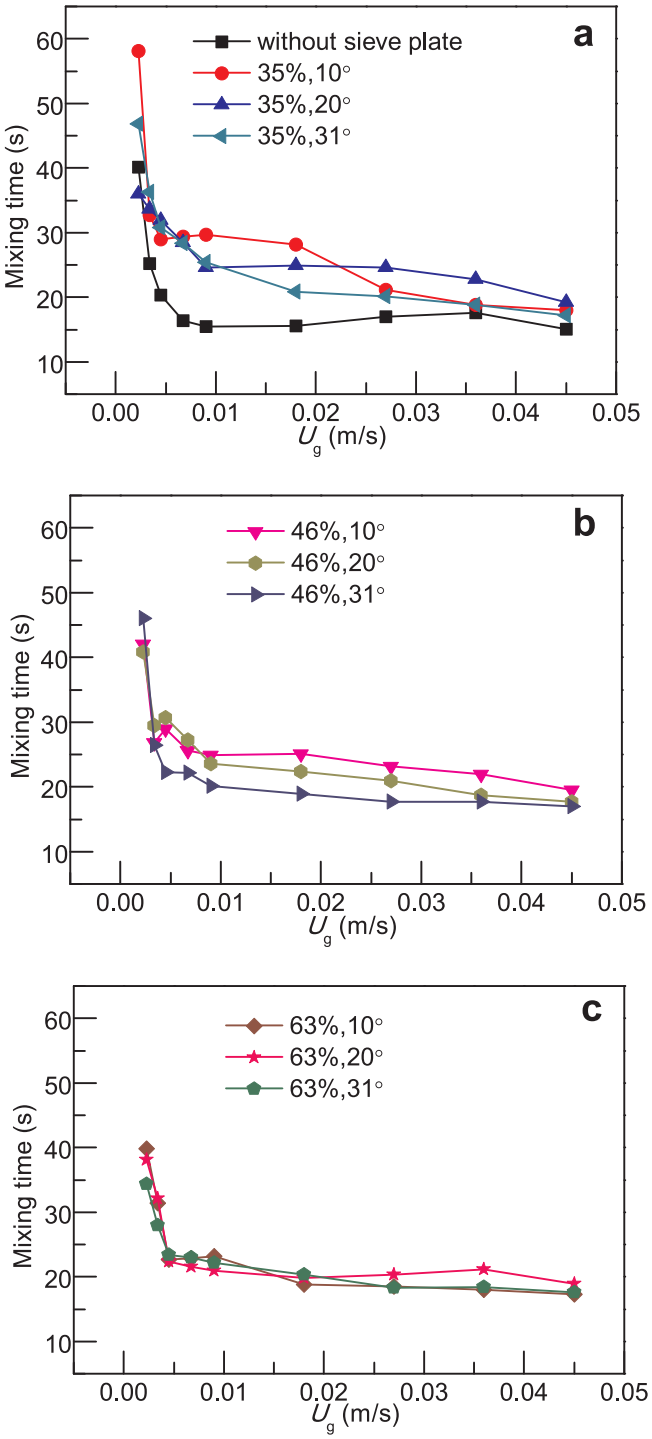

Fig. 9. Effect of superficial gas velocity on mixing time with different helical sieve plates. (a) ω = 35%; (b) ω = 46%; (c) ω = 63%.

3.4. Mixing time

Mixing time is also one of the key parameters for the design and scale-up of an ALR. In the present work, the tracer reagent (HCl solution) was added from the top of the reactor during the measurement of the mixing time. McClure et al. [38,39] found that the location of the tracer addition site had little effect on the mixing time. It was observed that the magenta color vanished in the bottom region slower than in the other regions. The overall mixing time was the duration time from the tracer addition to the completely vanishing of magenta color in the whole reactor. The axial mixing of ALR is mainly dependent on the velocity difference between the gas and liquid phases [40]. In the present work, the mixing in the top and bottom regions of the reactor was associated with the vortex flow formed by the HSP. Fig. 9 shows that the mixing time with the addition of the HSP was increased compared with that without sieve plate. The increase was due to the HSP partially impeding the gas–liquid fluid, thereby slowing down the liquid phase axial velocity. A similar result is previously obtained by adding a helical plate to the downcomer section of the ALR, thereby improving the tangential mixing performance [41,42]. Fig. 9a and b show that mixing time was reduced as the helix angle of the HSP increased. However, in Fig. 9c, mixing time was nearly constant as helix angle changed. It was concluded that when the high free area ratio was arranged in the HSP, the gas–liquid fluid flowed axially and the effect of helix angle on mixing time was weak.

Fig. 9 shows that mixing time decreased sharply when the $U_g < 0.01$ m/s, whereas it maintained a constant value when $U_g > 0.01$ m/s. This phenomenon was associated with the bubble rise velocity described by Haberman and Morton [43]. Since the bubble size in the reactor was concentrated in the range of 1.0–8.0 mm when the $U_g > 0.01$ m/s, both the bubble rising velocity and liquid velocity did not change obviously. It means that the mixing time does not depend on the U_g. Similar results were previously found for other ALRs [40]. In the current work, the oxygen transfer performance of ALR-HSP was enhanced mainly through the breakup of bubble and elongation of the gas–liquid contact time.

Compared with multi-layer OSPs, the HSPs enhanced the performance of gas–liquid mass transfer but decreased flow resistance and relieved the gas blocking. Furthermore, the new reactor widened the operating ranges and the flexibility.

4. Conclusions

The installation of an HSP in the riser can effectively intensify bubble breakup and reduce bubble size, thereby increasing gas holdup and volumetric mass transfer coefficient (k_La). The main reason for the increase of k_La is the increase in specific gas–liquid interfacial area (a). As the HSP leads the bubbles to rise upward helically, the bubbles will not accumulate under the sieve plate at high aeration rate. The circumferential velocity of bubbles increases with the increase in the helix angle of the plate but decreases with the increase in the free area ratio. The HSP causes even distribution of bubble size but extends the mixing time. The positive effect of the HSP on the mass transfer enhancement is much greater than the negative effect of the mixing slowdown.

Unlike cascaded bubble column with multi-layer OSPs, ALR-HSP has open entries at the upper and lower ends of the annular space between the draft tube and cylinder body. Cleaning and maintenance are easy and suitable for high hygiene and cleanliness requirements for microbial, animal, and plant cell cultures. The HSP will be washed by the upward rising gas–liquid flow in the helical direction and will not be easily blocked by growing bacteria or cell clusters. The new ALR can maintain efficient mass transfer performance and has potential for commercial biological cell culture.

Acknowledgements

Financial Support from Fundamental Research Funds for the Central Universities (JUSRP51632A, JUSRP51633B) and the Priority Academic Program Development of Jiangsu Higher Education Institutions, the 111 Project (No. 111-2-06) is gratefully acknowledged.

Appendix A. Supplementary data

Supplementary data associated with this article can be found, in the online version, at http://dx.doi.org/10.1016/j.cej.2018.01.039.

References

[1] Y. Chisti, W. Fu, M. Moo-Young, Relationship between riser and downcomer gas hold-up in internal-loop airlift reactors without gas-liquid separators, Chem. Eng. J. 57 (1995) B7–B13.

[2] J.C. Merchuk, M. Gluz, Bioreactors, air-lift reactors, in: M.C. Flickinger, S.W. Drew (Eds.), Encyclopedia of Bioprocess Technology, John Wiley & Sons Inc, New Jersey, 2002, pp. 1–61.

[3] M. del Carmen Oliver-Salvador, E. Morales-López, E. Durán-Páramo, C. Orozco-Álvarez, S. García-Salas, Shear rate and microturbulence effects on the synthesis of proteases by *Jacaratia mexicana* cells cultured in a bubble column, airlift, and stirred tank bioreactors, Biotechnol. Bioprocess. Eng. 18 (2013) 808–818.

[4] S.S.D. Jesus, J.M. Neto, R.M. Filho, Hydrodynamics and mass transfer in bubble column, conventional airlift, stirred airlift and stirred tank bioreactors, using viscous fluid: a comparative study, Biochem. Eng. J. 118 (2017) 70–81.

[5] K.S. Shin, H.N. Murthy, J.Y. Ko, K.Y. Paek, Growth and beta-cyanin production by hairy roots of *Beta vulgaris* in airlift bioreactors, Biotechnol. Lett. 24 (2002) 2067–2069.

[6] C.S. Lo, S.J. Hwang, Degradation of waste gas containing toluene in an airlift bioreactor, Environ. Sci. Technol. 38 (2004) 2271.

[7] T. Wang, J. Wang, Y. Jin, Slurry reactors for gas-to-liquid processes: a review, Ind. Eng. Chem. Res. 46 (2007) 5824–5847.

[8] A.B. Vakylabad, M. Schaffie, M. Ranjbar, Z. Manafi, E. Darezereshki, Bio-processing of copper from combined smelter dust and flotation concentrate: a comparative study on the stirred tank and airlift reactors, J. Hazard. Mater. 241 (2012) 197–206.

[9] A. Braga, D.P. Mesquita, A.L. Amaral, E.C. Ferreira, I. Belo, Aroma production by *Yarrowia lipolytica* in airlift and stirred tank bioreactors: differences in yeast metabolism and morphology, Biochem. Eng. J. 93 (2015) 55–62.

[10] S. Sharaf, M. Zednikova, M.C. Ruzicka, B.J. Azzopardi, Global and local hydrodynamics of bubble columns – effect of gas distributor, Chem. Eng. J. 288 (2016) 489–504.

[11] M. Räsänen, T. Eerikäinen, H. Ojamo, Characterization and hydrodynamics of a novel helix airlift reactor, Chem. Eng. Process. 108 (2016) 44–57.

[12] P. Rollbusch, M. Bothe, M. Becker, M. Ludwig, M. Grünewald, M. Schlüter, R. Franke, Bubble columns operated under industrially relevant conditions – current understanding of design parameters, Chem. Eng. Sci. 126 (2015) 660–678.

[13] W.B. Zimmerman, B.N. Hewakandamby, V. Tesař, H.C.H. Bandulasena, O.A. Omotowa, On the design and simulation of an airlift loop bioreactor with microbubble generation by fluidic oscillation, Food Bioprod. Process. 87 (2009) 215–227.

[14] Y. Chisti, M. Kasper, M. Moo-Young, Mass transfer in external-loop airlift bioreactors using static mixers, Can. J. Chem. Eng. 68 (1990) 45–50.

[15] M. Gavrilescu, R.V. Roman, A. Sauciuc, Oxygen mass transfer in an airlift bioreactor using static mixers, Biotechnol. Biotechnol. Equip. 6 (1992) 60–64.

[16] L. Luo, J. Yuan, P. Xie, J. Sun, W. Guo, Hydrodynamics and mass transfer characteristics in an internal loop airlift reactor with sieve plates, Chem. Eng. Res. Des. 91 (2013) 2377–2388.

[17] M. Zhao, K. Niranjan, J.F. Davidson, Mass transfer to viscous liquids in bubble columns and air-lift reactors: influence of baffles, Chem. Eng. Sci. 49 (1994) 2359–2369.

[18] N.L. Lukić, I.M. Šijački, P.S. Kojić, S.S. Popović, M.N. Tekić, D.L. Petrović, Enhanced mass transfer in a novel external-loop airlift reactor with self-agitated impellers, Biochem. Eng. J. 118 (2017) 53–63.

[19] B.R. Elbing, A.L. Still, A.J. Ghajar, Review of bubble column reactors with vibration, Ind. Eng. Chem. Res. 55 (2016) 385–403.

[20] J.R. Grace, T. Wairegi, J. Brophy, Break-up of drops and bubbles in stagnant media, Can. J. Chem. Eng. 56 (1978) 3–8.

[21] J. Liu, C. Zhu, T. Fu, Y. Ma, Systematic study on the coalescence and breakup behaviors of multiple parallel bubbles rising in power-law fluid, Ind. Eng. Chem. Res. 53 (2014) 4850–4860.

[22] X. Guo, Q. Zhou, J. Li, C. Chen, Implementation of an improved bubble breakup model for TFM-PBM simulations of gas–liquid flows in bubble columns, Chem. Eng. Sci. 152 (2016) 255–266.

[23] A.A. Avdeev, Bubble Systems, first ed., Springer International Publishing, Switzerland, 2016.

[24] V. Parisien, A. Farrell, D. Pjontek, C.A. McKnight, J. Wiens, A. Macchi, Bubble swarm characteristics in a bubble column under high gas holdup conditions, Chem. Eng. Sci. 157 (2017) 88–98.

[25] M. Ramezani, M.J. Legg, A. Haghighat, Z. Li, R.D. Vigil, M.G. Olsen, Experimental investigation of the effect of ethyl alcohol surfactant on oxygen mass transfer and bubble size distribution in an air-water multiphase Taylor-Couette vortex bioreactor, Chem. Eng. J. 319 (2017) 288–296.

[26] G. Besagni, F. Inzoli, Bubble size distributions and shapes in annular gap bubble column, Exp. Therm. Fluid Sci. 74 (2016) 27–48.

[27] R.A. Bello, C.W. Robinson, M. Moo-Young, Liquid circulation and mixing characteristics of airlift contactors, Can. J. Chem. Eng. 62 (2010) 573–577.

[28] R.A. Bello, C.W. Robinson, M. Moo-Young, Prediction of the volumetric mass transfer coefficient in pneumatic contactors, Chem. Eng. Sci. 40 (1985) 53–58.

[29] Y. Kawase, B. Halard, M. Moo-Young, Theoretical prediction of volumetric mass transfer coefficients in bubble columns for Newtonian and non-Newtonian fluids, Chem. Eng. Sci. 42 (1987) 1609–1617.

[30] X. Zhang, K. Guo, W. Qi, T. Zhang, C. Liu, Gas holdup, bubble behaviour, and mass transfer characteristics in a two-stage internal loop airlift reactor with different screens, Can. J. Chem. Eng. 96 (2017) 1002–1012.

[31] Z. Zheng, Y. Chen, X. Zhan, M. Gao, Airlift reactor assembly with helical sieve plate, US Patent (2017) App. No. 15,795,320.

[32] M. Nakanoh, F. Yoshida, Gas absorption by Newtonian and non-Newtonian liquids in a bubble column, Ind. Eng. Chem. Process Des. Dev. 19 (1980) 190–195.

[33] N. Kantarci, B.K.O. Ulgen, Bubble column reactors, Process Biochem. 36 (2005) 2263–2283.

[34] Y.T. Shah, B.G. Kelkar, S.P. Godbole, Design parameters estimations for bubble column reactors, AIChE J. 28 (1982) 353–379.

[35] T. Vorapongsathorn, P. Wongsuchoto, P. Pavasant, Performance of airlift contactors with baffles, Chem. Eng. J. 84 (2001) 551–556.

[36] M.R. Bhole, J.B. Joshi, D. Ramkrishna, CFD simulation of bubble columns incorporating population balance modeling, Chem. Eng. Sci. 63 (2008) 2267–2282.

[37] M.K.H. Al-Mashhadani, S.J. Wilkinson, W.B. Zimmerman, Airlift bioreactor for biological applications with microbubble mediated transport processes, Chem. Eng. Sci. 137 (2015) 243–253.

[38] D.D. McClure, T. Dolton, G.W. Barton, D.F. Fletcher, J.M. Kavanagh, Hydrodynamics and mixing in airlift contactors: Experimental work and CFD modelling, Chem. Eng. Res. Des. 127 (2017) 154–169.

[39] D.D. McClure, T.P. Dolton, G.W. Barton, D.F. Fletcher, J.M. Kavanagh, Mixing in bubble column reactors: experimental study and CFD modeling, Chem. Eng. J. 264 (2015) 291–301.

[40] P. Weiland, Influence of draft tube diameter on operation behavior of airlift loop reactors, Al-Khawarizmi Eng. J. 6 (2010) 374–385.

[41] M.D. Gluz, J.C. Merchuk, Modified airlift reactors: the helical flow promoters, Chem. Eng. Sci. 51 (1996) 2915–2920.

[42] C. Schlötelburg, M. Popovic, M. Gluz, J.C. Merchuk, Characterization of an airlift reactor with helical flow promoters, Can. J. Chem. Eng. 77 (1999) 804–810.

[43] W.L. Haberman, R.K. Morton, An experimental study of bubbles moving in liquids, ASCE 121 (1956) 227–250.